Pharmaceutical Research, Vol. 24, No. 4, April 2007 (© 2007)
DOI: 10.1007/s11095-006-9193-0

Research Paper

Isothermal Crystallization of Imwitor 742 from Supercooled Liquid State

Kohsaku Kawakami[1,2,3]

Received September 5, 2006; accepted November 14, 2006; published online February 15, 2007

PURPOSE. Crystallization behavior of Imwitor 742 was investigated for use as a liquid-filled capsule carrier.
MATERIALS AND METHODS. The crystallization behavior of Imwitor 742 was assessed using DSC, X-ray diffraction, and microscopy. The physical stability of Imwitor 742 under refrigerated and ambient conditions was estimated by isothermal crystallization studies using DSC. The effect of hard capsule shells and additives on crystallization kinetics was also examined.
RESULTS. When Imwitor 742 was cooled in the DSC measurement, the form α appeared at −20°C. When this form was heated from −40°C, melt-crystallization into the form β + β′ was initiated at −30°C, followed by successive melting. Isothermal crystallization studies at temperatures higher than −14°C yielded the form β + β′. The crystallization behavior was explained in terms of the Avrami model fitting by assuming 2-dimensional crystal growth. Kinetic analysis suggested that the liquid state of Imwitor 742 was maintained for 46 h and 40 months at 5 and 25°C, respectively, although the deviation in induction time was expected to be large at these temperatures. Addition of hard capsule shells promoted the crystallization behavior, while addition of drug or water prolonged the induction time.
CONCLUSION. The supercooled liquid state of Imwitor 742 was quite stable. However, additives to retard crystallization should be used, because the deviation in the induction time was very large. Hard capsule shells enhanced the crystallization of Imwitor 742, possibly by acting as nuclei for crystal growth.

KEY WORDS: crystallization; DSC; Imwitor 742; induction time; liquid-filled capsules.

INTRODUCTION

New chemical entities synthesized in pharmaceutical industries often possess poor aqueous solubility. Thus, there is great interest in studies on special dosage forms that promote drug dissolution. For example, use of amorphous state can improve the solubility of poorly soluble drugs (1, 2). Notably, the hot melt extrusion technology (2–4), which has been a common technique in the polymer industry (5), has increased chance of the amorphous formulation. The biggest problem associated with the amorphous formulation is, relatively poor physical/chemical stability (6,7). It may be overcome by understanding molecular mobility (8–10). Nevertheless, development of amorphous formulations remains a challenge for formulators.

Self-emulsifying formulation has also been an attractive option to improve absorption of drugs with poor aqueous solubility (11–14). The absorption mechanism of this formulation has been explained in terms of spontaneous formation of oil-in-water emulsion or microemulsion droplets in the stomach or small intestine. However, formation of such small droplets is not required to improve absorption in many cases, because simple oil formulations sometimes offer equivalent absorption behavior (14). Because addition of surfactants may cause toxicity (14), a simple oil formulation is better than the self-emulsifying formulation in such cases.

In this paper, the crystallization and melting behaviors of Imwitor 742, which is one of the candidates as a carrier for liquid-filled capsules, are described. Crystal forms of triacylglycerides have been investigated extensively to prove that there are three types of crystal forms, α, β, and β′(15–17). Figure 1 shows an energy-temperature diagram of these crystal forms with those structures, when the three acyl chain moieties are not similar each other. All of the crystal forms possess a lamellar type structure (17), and their thermodynamic relationship is monotropic (18–20), that is, the stability order does not depend on temperature below the melting point. The lamellar thickness of the form α is approximately equal to two times the length of the acyl chains, while those of the forms β and β′ are to three times. If the three acyl chains are identical or similar, the lamellar thickness of the forms β and β′ is equal to two times the length of the acyl chains as in the case of the form α. The same idea is valid for diglycerides, monoglycerides, and even mixtures of various glycerides (15).

The melting of Imwitor 742 occurs at ambient temperature. Therefore, it may crystallize during shipping or storage, if it is used as a drug carrier. Crystallization of Imwitor may not be a problem from absorption perspective,

[1] PreClinical Development, Banyu Tsukuba Research Institute, 3 Okubo, Tsukuba, Ibaraki, 300-2611, Japan.
[2] *Present address:* Biomaterials Center, National Institute for Materials Science, 1-1, Namiki, Tsukuba, Ibaraki, 305-0044, Japan.
[3] To whom correspondence should be addressed. (e-mail: kawakami.kohsaku@nims.go.jp)

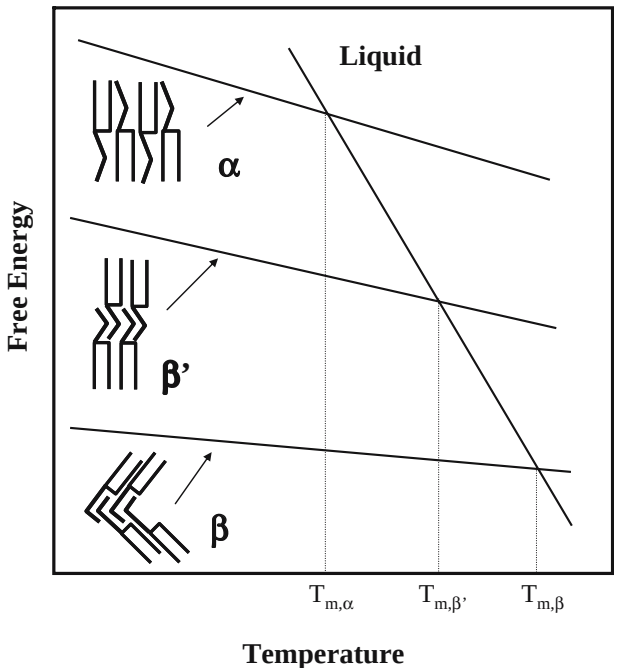

Fig. 1. A free energy-temperature diagram of acylglycerides. Structure shown in the figure is for the glycerides, each containing a different type of acyl chain. $T_{m,\alpha}$, $T_{m,\beta}$, and $T'_{m,\beta}$ are melting temperatures of the forms α, β, and β′, respectively.

because it should melt again after the oral administration. However, if drug molecules crystallize in the solid Imwitor, it may affect the absorption behavior. Another possible problem is that the crystallization of Imwitor may enable the discrimination of the drug-containing Imwitor from placebo formulations (i.e., pure Imwitor) in clinical studies, if the presence of the drug affects the crystallization behavior. This study was designed to evaluate how long the supercooled liquid state can be maintained and to examine its crystallization mechanism.

MATERIALS AND METHODS

Materials

Imwitor 742, which is a mixture of mono-/di-/tri-glycerides of caprylic and capric acids, was obtained from Sasol Germany GmbH (Witten, Germany). It is simply referred to as Imwitor hereafter. Imwitor was annealed at 50°C for 30 min to ensure a homogeneous liquid state before use, because it can solidify at ambient temperature. This process was always performed, even on the samples already in the liquid state before use. Gelatin and HPMC capsules were obtained from Capsugel (Morris Plains, NJ) and Qualicaps (Whitsett, NC), respectively. Other reagents were of the highest grade available and used as supplied.

Differential Scanning Calorimetry (DSC)

DSC studies were performed on a TA Q1000 (TA Instruments, New Castle, DE) calibrated with indium and sapphire. About 5 mg of Imwitor were loaded in an aluminum pan, followed by hermetical sealing with an aluminum lid. Preliminary studies using an open platinum pan showed that the crystallization behavior was not affected by sample volume in the range of 1–70 mg. Hermetical sealing of the pans did not affect the crystallization behavior of Imwitor, either. Before each run, samples were subjected to 10-min annealing at 50°C in the DSC cell. When this annealing temperature was lower than 40°C, very rapid crystallization was observed occasionally in isothermal crystallization studies, suggesting the existence of nuclei. Nitrogen was used as a purge gas at 50 ml/min.

Hot/cold Stage Microscopy

Hot/cold stage microscopy observation was performed on a Nikon OPTIPHOT 2-POL (Nikon, Tokyo, Japan) equipped with a Linkam THMS600 heating/freezing system (Linkam Scientific Instruments, Surrey, UK). A drop of Imwitor was introduced onto a glass plate, followed by gentle covering of the drop with a glass cover. Each observation was taken after annealing at 50°C for 10 min. Liquid nitrogen was used for cooling.

X-ray Diffraction (XRD)

An XRD measurement of the crystallized Imwitor was performed on an X'Pert Pro X-ray Diffraction System (PANalytical B. V., Almelo, The Netherlands). About 50 mg of Imwitor was loaded on a glass cell to store at −5°C for 2 h. Smooth surface was formed spontaneously during this crystallization process. Then, Imwitor was immediately transferred to the X-ray diffraction system to conduct a measurement under room temperature. This experimental procedure could provide sharper diffraction peaks than the *in-situ* crystallization study described next. The appearance of Imwitor did not change during the measurement. The voltage and the current were 45 kV and 40 mA, respectively. The X-ray data were collected between 1 and 40° (2 theta values) at intervals of 0.02° with a scan speed of 2.4°/min.

Simultaneous Measurement of X-ray Diffraction and DSC (XRD-DSC)

XRD-DSC measurements were performed on a Rigaku RINT X-ray Diffraction System with a Thermo Plus II DSC unit (Rigaku Denki, Tokyo, Japan). About 10 mg of Imwitor was assessed on a square-shaped aluminum pan. After 10-min annealing at 50°C for 10 min, Imwitor was cooled at 1.5°C/min to −20°C, followed by the cooling at 0.75°C/min to −40°C. Then, it was heated at 2°C/min up to 35°C. The voltage and the current were 40 kV and 40 mA, respectively. The X-ray data was collected between 16 and 30° (2 theta values) at intervals of 0.02° with a scan speed of 5°/min. It should be noted that the formation of the flat surface seemed to be difficult on aluminium pans, and thus this was the likely reason of the weakness and broadness of the diffraction peaks in this study.

HPLC Analysis

The chemical stability of Imwitor and possibility of elution from the capsule shells during the 50°C annealing

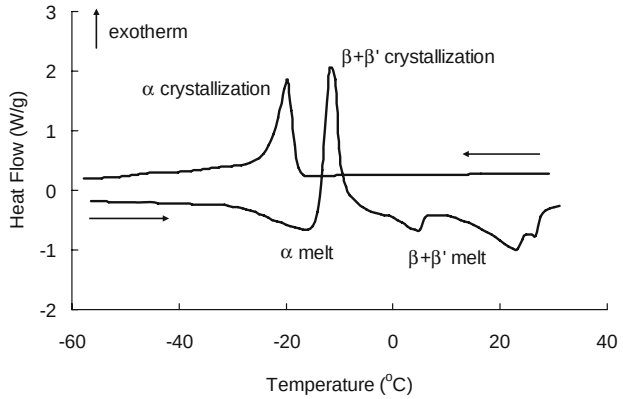

Fig. 2. A DSC thermogram of Imwitor. After annealing at 50°C, the sample was cooled at 10°C/min to −60°C, followed by a 3-min hold at −60°C and heating to 40°C at 10°C/min.

were assessed on an Agilent 1100 Series HPLC system (Agilent Technologies, Santa Clara , CA), because a trace amount of degradation or elution products may affect crystallization behavior. About 1 g of Imwitor was introduced to a glass tube, followed by incubation in a thermobath at 50°C for 30 min. About 200 mg of the shells were cut into small pieces and added to the tube to assess the possibility of elution. Incubated Imwitor with or without the capsule shell was diluted with ethanol to 100 μg/ml and subjected to HPLC analysis. Chromatograms were obtained using a YMC-pack Pro-C18 AS-302 (150 mmL × 4.6 mmID, YMC Co., Kyoto, Japan) at a flow rate of 1 ml/min. The column was equilibrated initially with 0.1% phosphoric acid/acetonitrile = 95/5. After 5 min, the mobile phase composition was linearly changed to 100% acetonitrile over 60 min, followed by elution by acetonitrile for 10 min. Detection wavelength and injection volume were 210 nm and 10 μl, respectively.

RESULTS AND DISCUSSION

Erasure of Thermal History: Annealing of Imwitor at 50°C

The annealing at 50°C for 10 min before each DSC measurement was found important to produce good reproducibility of crystallization behavior. Although the melting point of Imwitor was about 28°C, annealing below 40°C at durations shorter than 30 min was not sufficient, and led to poor reproducibility of crystallization behavior. In the HPLC study, the chromatogram contained many peaks, because Imwitor consisted of various glycerides. A 30-min incubation at 50°C did not affect the chromatograms. In addition, a 30-min incubation with gelatin or HPMC capsule shells at 50°C did not add any new peaks in the chromatograms. Thus, Imwitor appeared to be chemically stable at 50°C, and no elution from capsule shells seemed to occur during the annealing procedure.

Thermal Behavior of Imwitor

Figure 2 shows a DSC thermogram of Imwitor, of which the shape agreed very well with the thermogram for acyl glycerides in literature (15). The sharp peak occurring at −20°C during the cooling process could be elucidated in terms of the crystallization of the form α. During the heating

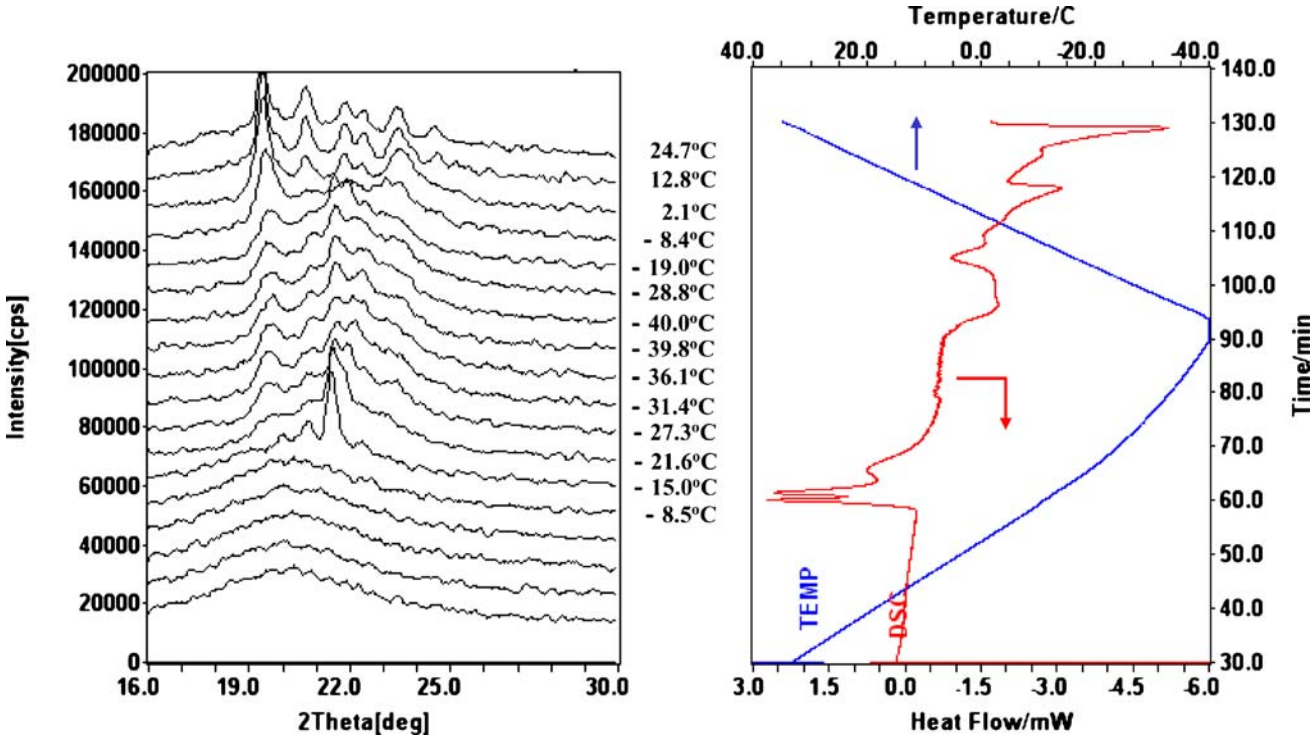

Fig. 3. XRD-DSC measurement of Imwitor. A *left figure* shows evolution of the X-ray diffraction pattern (*bottom* to *top*) during the cool-heat process. A *right figure* presents a thermal history with a thermogram. The temperature control below −20°C was not precise in the cooling process as can be seen in the temperature/time curve due to instrumental limitation. The temperature labels next to the diffractograms show the temperature at 30°.

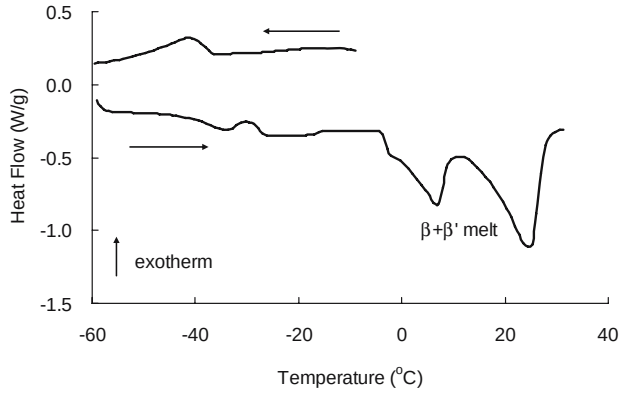

Fig. 4. A DSC thermogram of Imwitor after annealing at −5°C for 2 h. The sample was cooled at 10°C/min to −60°C, followed by a 3-min hold at −60°C and heating to 40°C at 10°C/min.

process, Imwitor melted at about −30°C, followed by the crystallization of the form β + β′. The forms β′ and β melted successively at about 0 and 15°C, respectively. The end point of the melting of the form β was about 28°C. Because the crystallization and the melting temperatures of the form α were consistent with each other, this temperature can be regarded as the equilibrium temperature between the form α and the liquid state. There was no indication of the transformation to the form β or β′ during the cooling process, although these forms are more stable than the form α. Figure 3 shows the result of XRD-DSC observation. It should be noted that the ramp rate for this study was much slower than that of the DSC study presented in Fig. 2. When Imwitor was cooled from the liquid state, a strong peak appeared at 21–22°, which was specific for the form α. The intensity of this peak decreased with decrease in the temperature. This was likely due to slow transformation to the form β + β′, and this seems to be a reasonable assumption because the form α is a less stable form in the entire temperature range. However, experimental artifacts may be involved as well, because the *in-situ* crystallization study could not provide smooth surface of the sample. After the melt-crystallization step in the heating process, the diffraction pattern became consistent with that of the form β + β′ (shown later). This evolution of the X-ray profile with the lapse of time was very similar to that for the melt-crystallization process from the forms α to β found in literature (17). During the cooling process, the crystallization exotherm into the form α split. The same was observed in the DSC study, when the sample was cooled at 2°C/min. The X-ray diffraction data suggest that this was due to partial transformation from the form α to β + β′. Although this observation indicates that the transition process was not as simple as that observed with small drug molecules, the form α was confirmed to occur first, followed by transition to the form β + β′ during the cooling/heating process.

Figure 4 shows a thermogram of the cooling/heating cycle at 10°C/min after annealing at −5°C for 2 h. The crystallization/melting peaks of the form α and the crystallization peak of the form β + β′ was not observed in this experiment, suggesting that the form β + β′ was obtained during annealing at −5°C. This was reasonable, because the melting temperature of the form α was assumed as below −20°C. Figure 5 shows an X-ray diffractogram of Imwitor after storing at −5°C for 2 h. Because the sharp peaks around 20° could be assigned to either that of the form β or β′ (15–17), Imwitor was most likely to crystallize into their mixture during the annealing.

Further insights in the thermal behavior of Imwitor were obtained through hot/cold stage microscopy. Figure 6 shows pictures obtained in the observation, where the same thermal program with that for Fig. 2 was applied. At about −16°C, feather-like structures appeared randomly from bulk (a), and the spaces between the solid phases were filled immediately by their growth (b). During the heating process, melting began at about −30°C with a dramatic decrease in the solid content before the temperature reached 0°C (c–d). Although the most likely explanation for this process was the melt-crystallization, re-crystallization to the forms β + β′ was not clearly observed in this study. The slow disappearance of the solid fraction was investigated in the following process (e–f) as can be expected from the DSC result. Figure 7 shows the pictures obtained in the observation, where the same thermal program with that for Fig. 4 was applied. In this case, crystallization was initiated from the edge of the view (a) and proceeded in a domino-like manner (b), suggesting that the energy barrier for the transformation from liquid structure to the form β + β′ was much larger than that to the form α. During the heating process, melting was not observed below 0°C (c), indicating the absence of the α form. The melting above 0°C was similar to the previous case but was slightly slower, probably due to the difference in the β/β′ ratio.

Isothermal Crystallization of Form β + β′

The crystallization of the form β + β′ is of a practical interest, because it can occur under standard storage conditions such as ambient or refrigerator temperatures. Thus, crystallization behavior of liquid Imwitor to the form β + β′ was observed using DSC under isothermal conditions. Figure 8 shows heat output during annealing at various temperatures. At temperatures lower than −12°C, a small peak was observed before the large crystallization peak in the DSC thermograms, probably due to crystallization of minor components or nucleation. Only the larger peaks were used

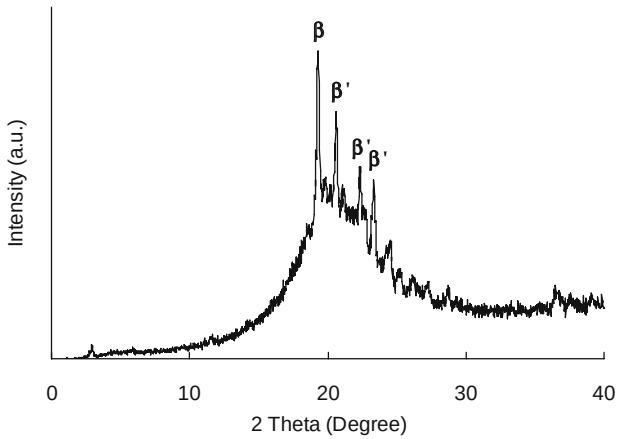

Fig. 5. An X-ray diffractogram of Imwitor crystallized at −5°C. The measurement was done under ambient condition. Every sharp peak was assigned as that of either form β or β′ as shown in the figure.

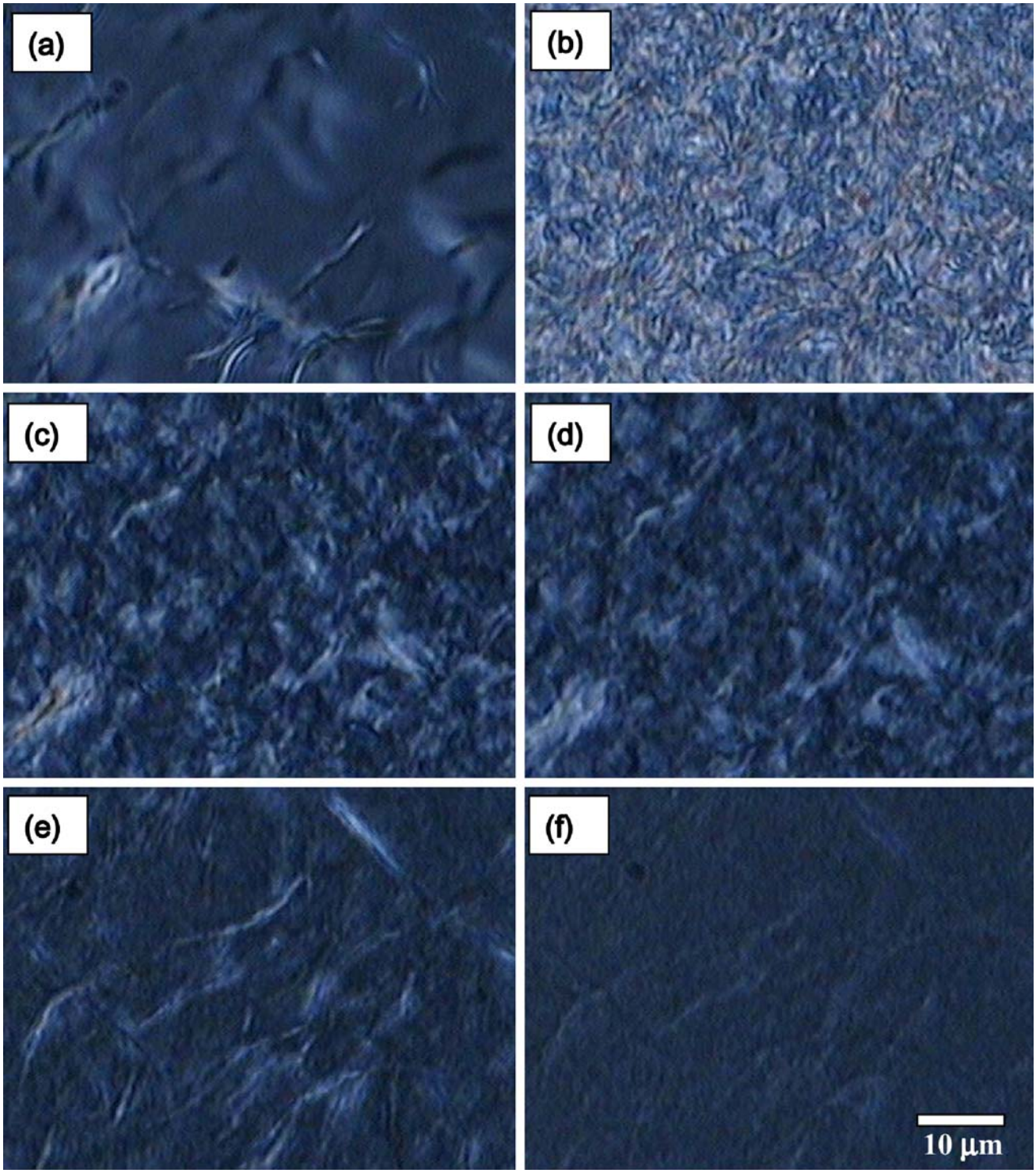

Fig. 6. Microscopic images of Imwitor in the hot/cold stage. After annealing at 50°C, the sample was cooled at 10°C/min to −60°C, followed by a 3-min hold at −60°C and heating to 40°C at 10°C/min. Pictures were obtained at (a) −16°C and (b) −40°C in the cooling process, and at (c) −12°C, (d) 0°C, (e) 6°C, and (f) 22°C in the heating process.

for kinetic analysis. At −10 and −8°C, although the crystallization process always began within 100 min, reproducibility of the shape of the thermograms was poor. At temperatures higher than −5°C, large variation in induction time was observed. Thus, initiation of the crystallization process seemed to depend on the arbitrary appearance of seed crystals. In other words, although the nucleation time was almost negligible at lower temperatures, its impact seemed to become very important with the increase in the crystallization temperature.

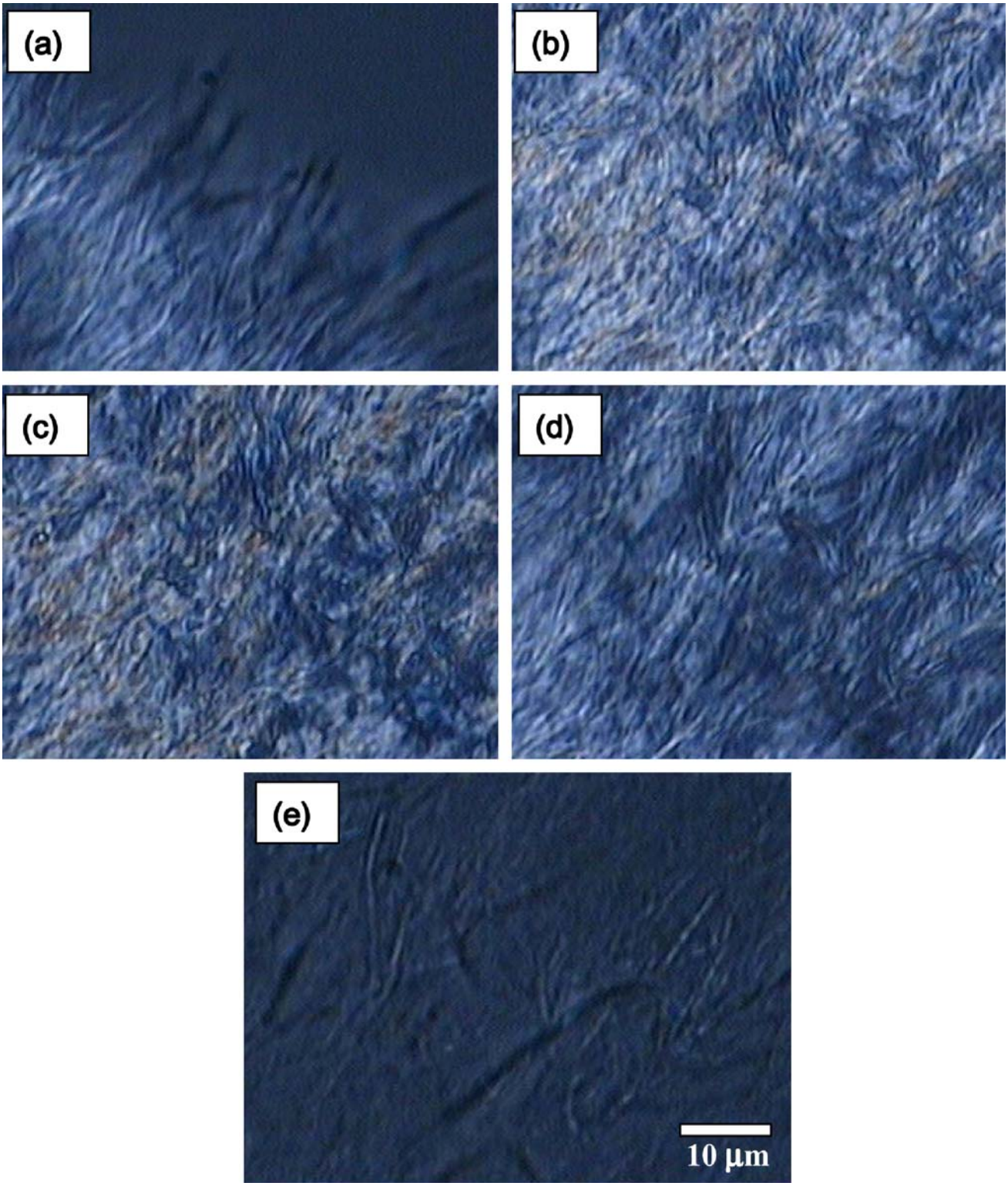

Fig. 7. Microscopic images of Imwitor in the hot/cold stage. After annealing at 50°C, the sample was subjected to isothermal crystallization at −5°C for 2 h. Then, the sample was cooled at 10°C/min to −60°C, followed by a 3-min hold at −60°C and heating to 40°C at 10°C/min. (a) was obtained during the isothermal crystallization after 90 min. Other pictures were obtained at (b) −20°C in the cooling process, and at (c) −20°C, (d) 10°C, and (e) 26°C in the heating process.

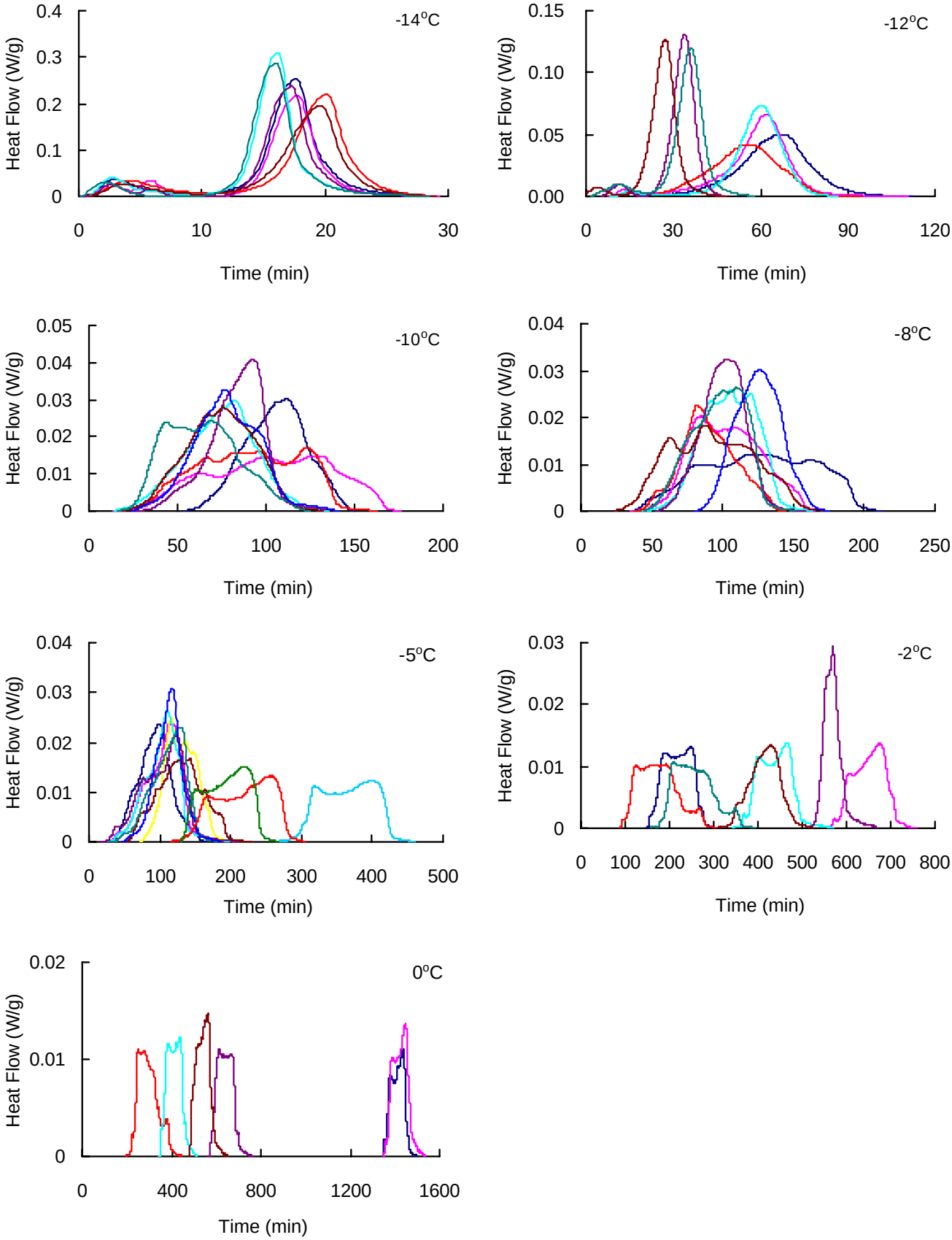

Fig. 8. Heat flow generated during the isothermal crystallization observed by DSC. The sample size was about 5 mg. The same measurement was repeated at least six times, each differentiated by a different color (in the case of the on-line journal). The crystallization temperatures were presented in the figures.

Table I. Solid-state Reaction Models in their Integral Forms

Notation	Reaction Mechanism	$g(\alpha)$
A2	Avrami-Erofeev, $n=2$	$(-\ln(1-\alpha))^{1/2}$
A3	Avrami-Erofeev, $n=3$	$(-\ln(1-\alpha))^{1/3}$
A4	Avrami-Erofeev, $n=4$	$(-\ln(1-\alpha))^{1/4}$
D1	One-dimensional diffusion	α^2
D2	Two-dimensional diffusion	$(1-\alpha)\ln(1-\alpha)+\alpha$
D3	Three-dimensional diffusion (Jander)	$(1-(1-\alpha)^{1/3})^2$
D4	Three-dimensional diffusion (Ginstling–Brounshtein)	$1-2\alpha/3-(1-\alpha)^{2/3}$
F1	First-order reaction (Mampel)	$-\ln(1-\alpha)$
F2	Second-order reaction	$1/(1-\alpha)-1$
PL2	Power law ($n=1/2$)	$\alpha^{1/2}$
PL3	Power law ($n=1/3$)	$\alpha^{1/3}$
PL4	Power law ($n=1/4$)	$\alpha^{1/4}$
R1	One-dimensional phase boundary reaction (zero-order)	α
R2	Two-dimensional phase boundary reaction	$1-(1-\alpha)^{1/2}$
R3	Three-dimensional phase boundary reaction	$1-(1-\alpha)^{1/3}$

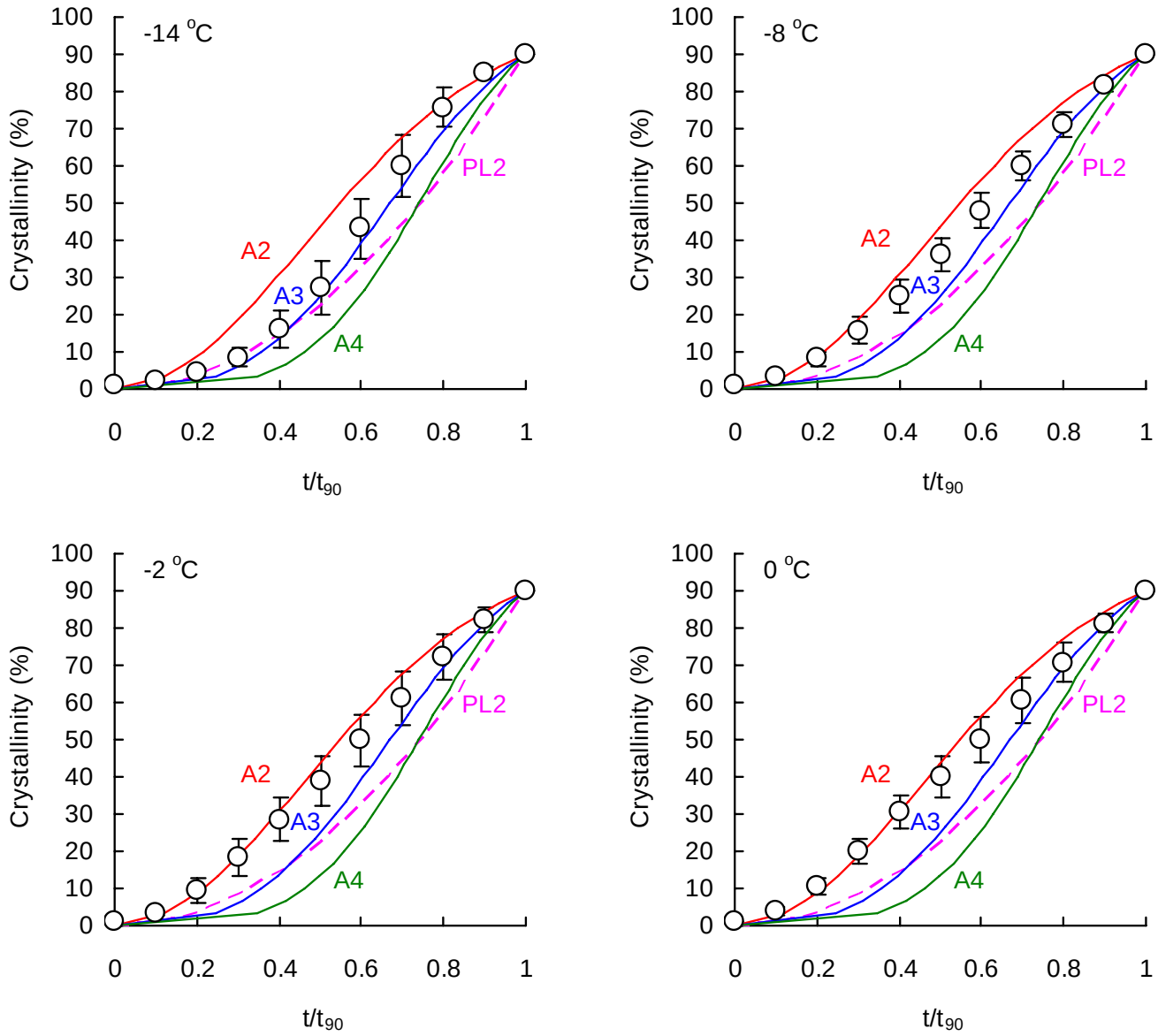

Fig. 9. Examples of reduced-time plots of isothermal crystallization. Averaged values of all the runs are presented with *error bars* indicating standard deviations. Representative evolution *curves*, of which the shapes are similar to the raw data, are also shown.

Table II. Theoritical Meanings of Avrami Exponents (26, 27)

Crystallization Mechanism	Dimension of Growth		
	3	2	1
Homogeneous nucleation (constant nucleation rate) Surface controlled growth (constant growth rate)	4	3	2
Homogeneous nucleation (constant nucleation rate) Diffusion controlled growth	2.5	2	1.5
Heterogeneous nucleation (decreasing nucleation rate) Surface controlled growth (constant growth rate)	3	2	1
Heterogeneous nucleation (decreasing nucleation rate) Diffusion controlled growth	1.5	1	0.5

Kinetic Analysis

The kinetic equation of the crystallization process is generally described as

$$\frac{d\alpha}{dt} = k(T)f(\alpha) \tag{1}$$

where α and t are the fraction crystallized and the elapsed time, respectively (21). The rate constant k, as a function of the temperature T, can be separated from the reaction model equation $f(\alpha)$. Under isothermal conditions, nucleation and crystal growth can be regarded as proceeding simultaneously. Thus, Eq. 1 can be transformed as

$$g(\alpha) = \int_0^\alpha \frac{d\alpha}{f(\alpha)} = k(T)t \tag{2}$$

The representative reaction models in the form of $g(\alpha)$, which is an integrated form of $f(\alpha)^{-1}$, are shown in Table I. The most common approach to select the appropriate model has been to analyze the data using all models and make a selection on a statistical basis, that is, goodness of fit. However, this approach may be problematic (21–23), because usually several models give a good fit without statistically meaningful differences among the models. Also, the reaction mechanism may change during the reaction (24), which can lead to incorrect selection of the reaction model. Therefore, the reduced time plot (21,25) was employed first to select the adequate reaction model.

Figure 9 shows examples of the reduced-time plot. The reduced-time t/t_{90} was defined as the elapsed time divided by the 90% crystallization time without including the induction period. The crystallization mechanism was well described by the A3 equation for the run at −14°C. Interestingly, the mechanism shifted toward A2 with an increase in crystallization temperature. Table II shows a summary of the theoretical meaning of the Avrami exponent (26,27). Two explanations for the decrease in the Avrami exponent are possible: a decrease in the dimension of growth or a change in the nucleation/growth mechanism. Because the induction time is dominated by the nucleation process, it is obvious that the nucleation rate significantly decreased with an increase in crystallization temperature. Thus, the drastic difference in the nucleation rate may be regarded as the difference in the nucleation mechanism (i.e., homogeneous or heterogeneous) in the overall crystallization process. As for the dimension of growth, the most natural assumption is 2-dimensional growth, because the crystal structure of Imwitor is of lamellar type. Therefore, the most likely interpretation for the change in the Avrami exponent with an increase in temperature is a change in the crystallization mechanism from homogeneous to heterogeneous nucleation under the assumption of the surface-controlled 2-dimensional growth.

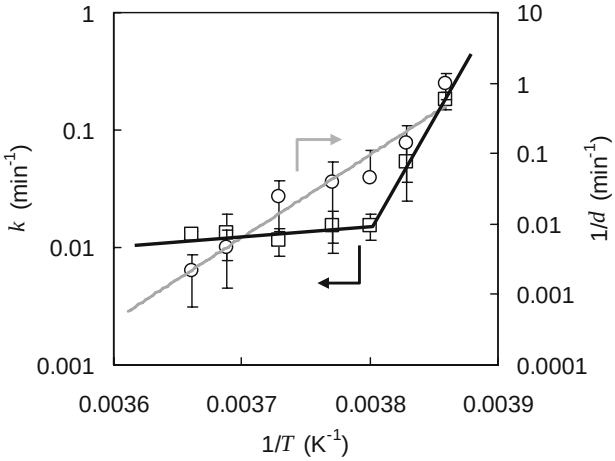

Fig. 10. Time dependence of crystallization rate k (*circles*) and induction time d (*squares*).

Figure 10 shows the temperature dependence of the rate constant k and induction time d obtained form the Avrami fitting. The temperature dependence of the rate constant was very strong below −10°C, however, it was nearly constant above that. This is most likely related to the presence of the small pre-peak in the thermograms below −12°C (Fig. 8). The unidentified substance, produced in a very short time, seemed to help the subsequent crystallization. Because crystallization rate did not depend much on temperature above −10°C, the factor influencing crystallization time will be the induction time, which is heavily dependent on temperature throughout the entire range investigated. Extrapolation of the results indicated that the time required for crystallization was about 46 h and 40 months at 5 and 25°C, respectively. Note, however, that the deviation in induction time became very large with an increase in temperature. Thus, it may not be adequate to conclude that the liquid state of Imwitor 742 can be maintained for 40 months at room temperature.

Table III. Crystallization Parameters at −10°C w/ or w/o Additives

	n	k (min^{-1})	d (min)
No additives	3	0.015 ± 0.004	21.8 ± 19.2
+HPMC shell	2	0.035 ± 0.001	24.1 ± 3.3
+Gelatin shell	2	0.030 ± 0.006	28.5 ± 5.6
+5% MK-5435	2	0.019 ± 0.002	43.2 ± 8.7
+5% Water	2	0.014 ± 0.001	105.2 ± 37.4

Effect of Capsule Shells and Additives

Table III shows the crystallization parameters obtained at −10°C in the presence of the capsule shells, drug (MK-5435), or water. The presence of the capsule shells enhanced the crystallization behavior by increasing the crystallization rate regardless of the material. Because the Avrami exponent was also affected by the shells, they may act as nuclei. Significant improvement in reproducibility of the crystallization behavior, indicated by small standard deviations, may be evidence of this hypothesis as well. In contrast, addition of drug or water prolonged induction time. The DSC measurement revealed that the melting temperature was hardly affected by these additives, indicating that they were likely to act as impurities to inhibit crystallization physically. Because it seems to be difficult to ensure maintenance of the liquid state of Imwitor over a period of several years, the crystallization behavior should be controlled by additives for the use of a liquid-filled capsule carrier. Thus, it is recommended to mix liquid surfactant such as Tween or Chremophor or oils with higher melting temperatures with Imwitor, when it was used as a liquid carrier.

CONCLUSION

Crystallization behavior of Imwitor was investigated for use as a liquid-filled capsule carrier. When Imwitor was cooled in the DSC measurement, the form α appeared at −20°C. During the heating process, melt-crystallization into the form $\beta+\beta'$ began at −30°C, followed by successive melting of these forms. Isothermal crystallization studies above −14°C yielded the form $\beta+\beta'$. The crystallization behavior was explained in terms of the Avrami model fitting by assuming 2-dimensional crystal growth. The kinetic analysis suggested that the liquid state of Imwitor 742 may be maintained for 46 h and 40 months at 5 and 25°C, respectively. Addition of hard capsule shells promoted the crystallization behavior, while addition of drug or water prolonged induction time. Additives to retard crystallization should be used, because the deviation in the induction time was so large that the reproducible crystallization time cannot be expected.

REFERENCES

1. S. Byrn, R. Pfeiffer, M. Ganey, C. Hoiberg, and G. Poochikian. Pharmaceutical solids: a strategic approach to regulatory considerations. *Pharm. Res.* **12**:945–954 (1995).
2. A. T. M Serajuddin. Solid dispersion of poorly-soluble drugs: early promises, subsequent problems, and recent breakthroughs. *J. Pharm. Sci.* **88**:1058–1066 (1999).
3. N. Follonier, E. Doelker, and E. T. Cole. Evaluation of hot-melt extrusion as a new technique for the production of polymer-based pellets for sustained release capsules containing high loadings of freely soluble drugs. *Drug Dev. Ind. Pharm.* **20**: 1323–1339 (1994).
4. J. Breitenbach. Melt extrusion: from process to drug delivery technology. *Eur. J. Pharm. Biopharm.* **54**:107–117 (2002).
5. J. L. White, W. Szydlowski, K. Min, and M. H. Kim. Twin screw extruders; development of technology and analysis of flow. *Adv. Polymer. Tech.* **7**:295–332 (1987).
6. Y. Guo, S. R. Byrn, and G. Zografi. Physical characteristics and chemical degradation of amorphous quinapril hydrochloride. *J. Pharm. Sci.* **89**:128–143 (2000).
7. S. R. Byrn, W. Xu, and A. W. Newman. Chemical reactivity in solid-state pharmaceuticals: formulation implications. *Adv. Drug Deliv. Rev.* **48**:115–136 (2001).
8. L. Yu. Amorphous pharmaceutical solids: preparation, characterization and stabilization. *Adv. Drug Deliv. Rev.* **48**:27–42 (2001).
9. D. Zhou, G. G. Z. Zhang, D. Law, D. J. W. Grant, and E. A. Schmitt. Physical stability of amorphous pharmaceuticals: importance of configurational thermodynamic quantities and molecular mobility. *J. Pharm. Sci.* **91**:1863–1872 (2002).
10. K. Kawakami and M. J. Pikal. Calorimetric investigation of the structural relaxation of amorphous materials: Evaluating validity of the methodologies. *J. Pharm. Sci.* **94**:948–965 (2005).
11. P. Erkko, H. Granlund, M. Nuutinen, and S. Reitamo. Comparison of cyclosporine A pharmacokinetics of a new microemulsion formulation and standard oral preparation in patients with psoriasis. *Br. J. Dermatol.* **136**:82–88 (1997).
12. M. J. Lawrence and G. D. Rees. Microemulsion-based media as novel drug delivery systems. *Adv. Drug Deliv. Rev.* **45**:89–121 (2000).
13. K. Kawakami, T. Yoshikawa, Y. Moroto, E. Kanaoka, K. Takahashi, Y. Nishihara, and K. Masuda. Microemulsion formulation for enhanced absorption of poorly soluble drugs. I. Prescription design. *J. Control. Release* **81**:65–74 (2002).
14. K. Kawakami, T. Yoshikawa, T. Hayashi, Y. Nishihara, and K. Masuda. Microemulsion formulation for enhanced absorption of poorly soluble drugs. II. *In vivo* study. *J. Control. Release* **81**:75–82 (2002).
15. J. W. Hagemann. Thermal behavior and polymorphism of acylglycerides. In *Crystallization and Polymorphism of Fats and Fatty Acids*. Marcel Dekker, New York, 1989.
16. R. E. Timms. Phase behaviour of fats and their mixtures. *Prog. Lipid Res.* **23**:1–38 (1984).
17. K. Sato. Crystallization behaviour of fats and lipids—a review. *Chem. Eng. Sci.* **56**:2255–2265 (2001).
18. L. Yu. Inferring thermodynamic stability relationship of polymorphs from melting data. *J. Pharm. Sci.* **84**:966–974 (1995).
19. D. Giron. Investigations of polymorphism and pseudo-polymorphism in pharmaceuticals by combined thermoanalytical techniques. *J. Therm. Anal. Calorim.* **64**:37–60 (2001).
20. K. Kawakami. Reversibility of enantiotropically-related polymorphic transformations from a practical viewpoint: thermal analysis of kinetically reversible/irreversible polymorphic transformations. *J. Pharm. Sci.* (in press).
21. K. Kawakami, K. Miyoshi, N. Tamura, T. Yamaguchi, and Y. Ida. Crystallization of sucrose glass under ambient conditions: evaluation of crystallization rate and unusual melting behavior of resultant crystals. *J. Pharm. Sci.* **95**:1354–1363 (2006).
22. H. S. Ray. Some factors that lead to uncertainties in kinetic studies in metallurgy. *J. Therm. Anal.* **36**:743–764 (1990).
23. M. T. Ledwidge and O. I. Corrigan. Effects of environmental factors on the dehydration of diclofenac HEP dihydrate and theophylline monohydrate. *Int. J. Pharm.* **147**:41–49 (1997).
24. D. Zhou, E. A. Schmitt, G. G. Zhang, D. Law, S. Vyazovkin, C. A. Wight, and D. J. W. Grant. Crystallization kinetics of amorphous nifedipine studied by model-fitting and model-free approaches. *J. Pharm. Sci.* **92**:1779–1792 (2003).
25. S. Vyazovkin and C. A. Wight. Isothermal and nonisothermal reaction kinetics in solids: in search of ways toward consensus *J. Phys. Chem., A* **101**:8279–8284 (1997).
26. E. D. Zanotto. The applicability of the general theory of phase transformations to glass crystallization. *Thermochim. Acta* **280/281**:73–82 (1996).
27. S. Sakka. *Garasu Kagaku no Kiso to Ouyou*, 2nd ed. (in Japanese). Uchida Rokakuho Publishing, Tokyo, 2000.